

Secondary instability in the wake of a circular cylinder

Ronald D. Henderson Dwight Barkley

Citation: *Physics of Fluids* **8**, 1683 (1996); doi: 10.1063/1.868939

View online: <http://dx.doi.org/10.1063/1.868939>

View Table of Contents: <http://aip.scitation.org/toc/phf/8/6>

Published by the [American Institute of Physics](#)

Articles you may be interested in

[Three-dimensional transition of vortex shedding flow around a circular cylinder at right and oblique attacks](#)

Physics of Fluids **25**, 014105 (2013); 10.1063/1.4788934

[On the transition of the cylinder wake](#)

Physics of Fluids **7**, 779 (1998); 10.1063/1.868601

COMPLETELY

REDESIGNED!



**PHYSICS
TODAY**

Physics Today Buyer's Guide
Search with a purpose.

Secondary instability in the wake of a circular cylinder

Ronald D. Henderson

Aeronautics and Applied Mathematics, California Institute of Technology, Pasadena, California 91125

Dwight Barkley

Nonlinear Systems Laboratory, Mathematics Institute, University of Warwick, Coventry, CV4 7AL, United Kingdom

(Received 7 December 1995; accepted 9 February 1996)

Secondary instability of flow past a circular cylinder is examined using highly accurate numerical methods. The critical Reynolds number for this instability is found to be $Re_c = 188.5$. The secondary instability leads to three-dimensionality with a spanwise wavelength at onset of 4 cylinder diameters. Three-dimensional simulations show that this bifurcation is weakly subcritical. © 1996 American Institute of Physics. [S1070-6631(96)00906-1]

The von Kármán vortex street generated by flow past a circular cylinder is, at low Reynolds numbers and under ideal conditions, a perfectly time-periodic, two-dimensional flow. This periodic state develops from steady flow at the primary wake instability, now well-characterized and known to correspond to a supercritical Hopf bifurcation.^{1,2} Subsequent instabilities in the cylinder wake have been given attention only recently and they are still not adequately understood. In this Brief Communication we discuss the use of highly accurate computational methods to explore the secondary instability in the cylinder wake. This is a global three-dimensional instability of the two-dimensional, time-periodic vortex street. From a combination of linear and nonlinear computations we derive quantitative data about the bifurcation (such as critical Reynolds number and critical spanwise wavelength) as well as insight into the qualitative nature of the transition.

Our computational approach is summarized as follows. First we perform direct simulations of the incompressible Navier–Stokes equations to obtain 2-D wake flows for $140 \leq Re \leq 300$, where Re is the Reynolds number defined by $Re \equiv U_\infty d / \nu$; U_∞ is the free-stream velocity far from the cylinder, d is the cylinder diameter, and ν is the kinematic viscosity. For the 2-D simulations we use a spectral element method with high resolution on large computational domains: meshes have 170 to 300 elements and a polynomial basis of sixth to tenth order. The unsteady solution is integrated until it reaches an asymptotic time-periodic state $\mathbf{U}(x, y, t)$, that is $\mathbf{U}(x, y, t + T) = \mathbf{U}(x, y, t)$ where T is the wake period (one shedding cycle). These periodic flows are then stored for use in our stability calculations.

The second step of our method is a Floquet stability analysis of 3-D disturbances to the 2-D wake. Consider an infinitesimal perturbation of the 2-D flow given by

$$\mathbf{u}(x, y, z, t) = \mathbf{U}(x, y, t) + \mathbf{u}'(x, y, z, t). \quad (1)$$

Ignoring terms quadratic in \mathbf{u}' , the evolution of perturbations is determined by the Navier–Stokes equations linearized about \mathbf{U} :

$$\frac{\partial \mathbf{u}'}{\partial t} = -(\mathbf{U} \cdot \nabla) \mathbf{u}' - (\mathbf{u}' \cdot \nabla) \mathbf{U} - \frac{1}{\rho} \nabla p' + \frac{1}{Re} \nabla^2 \mathbf{u}', \quad (2)$$

where p' is the perturbation to the pressure that enforces $\nabla \cdot \mathbf{u}' = 0$.

Floquet theory applies to linear differential equations with time-periodic coefficients, in this case Eq. (2) with coefficients given by \mathbf{U} . In the absence of degeneracies, the general solution can be expressed as a sum of solutions of the form $\tilde{\mathbf{u}}(x, y, z, t) \exp(\sigma t)$, where σ is a Floquet exponent and each Floquet mode $\tilde{\mathbf{u}}$ is a T -periodic function. Stability of \mathbf{U} is characterized by the spectrum of Floquet multipliers, $\mu \equiv \exp(\sigma T)$: exponentially growing perturbations correspond to multipliers outside the unit circle in the complex plane ($|\mu| > 1$).

Because the cylinder is homogeneous in the spanwise direction z , the Floquet modes must be of the form

$$\tilde{\mathbf{u}}(x, y, z, t) = (\hat{u} \cos \beta z, \hat{v} \cos \beta z, \hat{w} \sin \beta z), \quad (3)$$

or an equivalent form obtained by translation in z , where β is the spanwise wave number and \hat{u} , \hat{v} , and \hat{w} are functions of (x, y, t) only. In this way the 3-D stability problem for fixed Re reduces to a one-parameter family of 2-D stability problems that depend on β . We integrate Eq. (2) using a method similar to that used to compute \mathbf{U} , and employ a Krylov method to find the dominant Floquet multiplier and corresponding Floquet mode as a function of the parameters Re and β . A more detailed description of our numerical method is described in Ref. 3.

Figure 1 shows the dependence of the dominant Floquet multiplier on spanwise wave number β for values of Re encompassing the secondary instability. For each Re there is a Floquet multiplier $\mu = 1$ at $\beta = 0$ because autonomous time-periodic flows always have a neutrally-stable Floquet mode of the form $\tilde{\mathbf{u}}_T \propto \partial \mathbf{U} / \partial t$.⁴ This is a 2-D mode ($\beta = 0$) because \mathbf{U} is a 2-D flow. For $Re = 140$, the leading multiplier decreases monotonically as a function of β . At $Re = 170$, this multiplier branch has a local maximum at finite β . The height of this maximum grows and shifts to a slightly higher wave number as Re increases, reaching $\mu = 1$ at the critical values for the secondary instability: $Re_c = 188.5$, $\beta_c = 1.585$. The critical wavelength $\lambda_c = 2\pi / \beta_c$ corresponds to almost exactly 4 cylinder diameters. These values compare quite well with experimental observations discussed in the companion article by Williamson.⁵ For $Re > Re_c$ there is a band

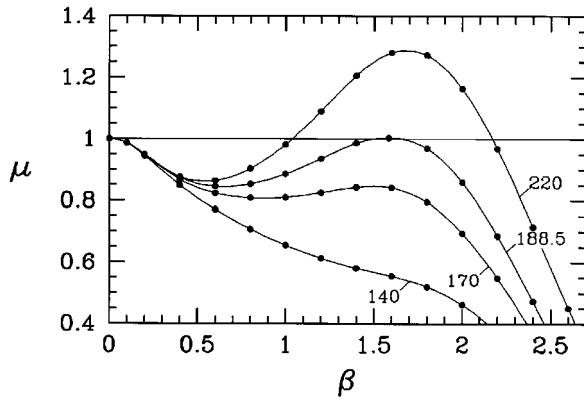


FIG. 1. Dependence of the dominant Floquet multiplier on spanwise wave number for values of Re indicated. Multipliers are real and positive, and each branch is symmetric: $\mu(\beta) = \mu(-\beta)$.

of unstable wave numbers corresponding to $\mu > 1$. By computing this band at different values of Re we obtain the neutral-stability curve shown in Fig. 2.

We now turn to the nonlinear classification of the secondary instability. For this we consider the normal form for a pitchfork bifurcation of a discrete-time dynamical system:

$$A_{n+1} = \mu A_n + \alpha_1 A_n^3 + O(A_n^5), \quad (4)$$

where A_n corresponds to the (real) amplitude of the bifurcating flow at period n and α_1 is called the Landau constant. If $\alpha_1 < 0$, the instability is a *supercritical* (soft) bifurcation. If $\alpha_1 > 0$, the instability is a *subcritical* (hard) bifurcation: transition is discontinuous and hysteretic.

To determine the nonlinear character of the secondary instability, we performed direct simulations near Re_c using the full 3-D Navier–Stokes equations. The most precise and direct way to analyze the nonlinear growth of the critical mode is to follow the evolution of initial conditions of the form $\mathbf{U} + \hat{\mathbf{u}}_c$, where $\hat{\mathbf{u}}_c$ is a Floquet mode at β_c . Moreover, because the Navier–Stokes equations preserve the subspace of 3-D solutions spanned by wave numbers $m\beta_c$ for integers

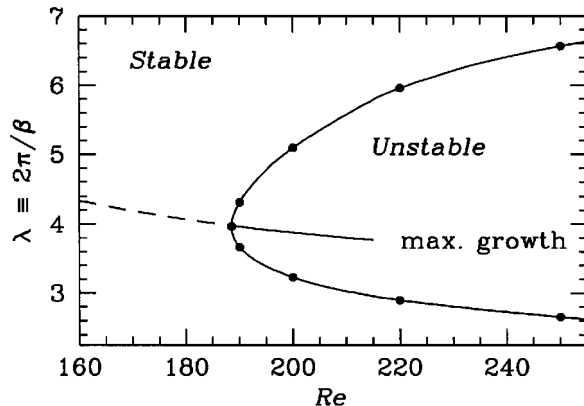


FIG. 2. Neutral-stability curve for the cylinder wake. Everywhere to the right of the curve there exist exponentially growing 3-D Floquet modes with the indicated wavelength; the dashed–solid line indicates the mode with the maximum linear growth rate.

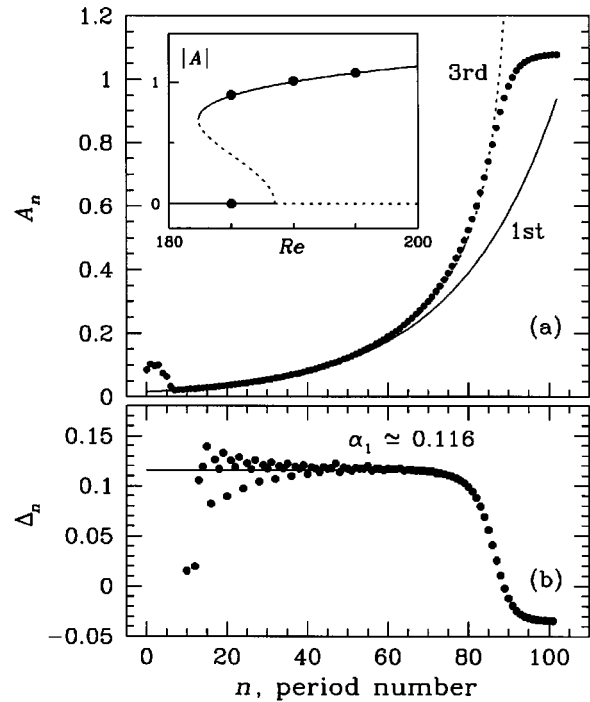


FIG. 3. Nonlinear character of the secondary instability. (a) A_n from 3-D simulation at $Re = 195$ (points). Curves show results from the normal form at first and third order with $\mu = 1.041$ and $\alpha_1 = 0.116$. (b) Δ_n computed from the data in (a) showing $\alpha_1 > 0$ and therefore that the secondary instability is subcritical. The inset shows a bifurcation diagram based on the normal form together with asymptotic states from 3-D simulations (points).

m , it is sufficient to retain only these modes when the initial condition lies in this subspace. In our simulations we retained all modes with $|m| \leq M = 16$.

We define the amplitude A_n of the 3-D flow after n periods (shedding cycles) by

$$A_n \equiv \left[\frac{4}{\pi d^2 U_\infty^2} \int_{\Omega} |\hat{\mathbf{u}}_c|^2 d\Omega \right]^{1/2}, \quad (5)$$

where Ω is the 2-D cross-section of the computational domain and $\hat{\mathbf{u}}_c(x, y, t_n)$ is the Fourier coefficient of the velocity field at period (or shedding cycle) n and wave number β_c . To determine the value of α_1 , we analyze A_n in the neighborhood of the critical point $(1 + \epsilon)Re_c$, where $\epsilon \equiv (Re - Re_c)/Re_c$ is a small parameter.

Figure 3(a) shows the result of a 3-D simulation at $Re = 195$ ($\epsilon = 0.03$). Near the point of saturation, A_n departs from the exponential growth described by $A_{n+1} = \mu A_n$. Initially this departure is governed by the third-order term in (4). One can quantify the deviation by evaluating

$$\Delta_n \equiv (A_{n+1} - \mu A_n) / A_n^3,$$

which according to the normal form is $\Delta_n = \alpha_1 + O(A_n^2)$. This is plotted in Fig. 3(b). Although at low amplitudes Δ_n fluctuates considerably, its mean value is almost constant until the $O(A_n^5)$ term in (4) becomes important. From the data we estimate $\alpha_1 \approx 0.116$. Figure 3(a) shows the growth curve from the normal form truncated at third order. Excel-

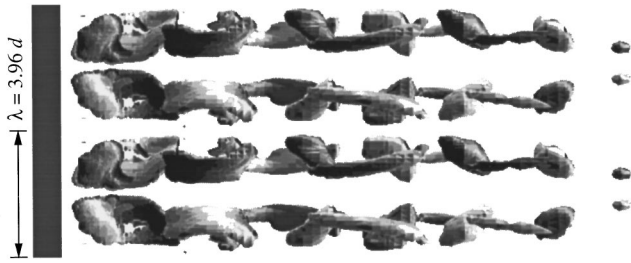


FIG. 4. Visualization of the streamwise vorticity field for the saturated state at $Re=195$. Light and dark surfaces correspond to positive and negative streamwise vorticity with a magnitude of $|\xi_x d/U_\infty|=0.75$.

lent agreement between the simulation data and the third-order normal form with positive α_1 clearly indicates that the secondary instability is subcritical.

To strengthen this conclusion we performed additional 3-D simulations at $Re=185$ and 190 . At $Re=190$ ($\epsilon=0.008$), we again found $\alpha_1 \approx 0.116$. Below the critical point at $Re=185$ we found bi-stability between the 2-D flow ($A=0$) and a 3-D flow ($A \neq 0$): initial conditions corresponding to $A_0=0.1$ decayed back to zero, while initial conditions corresponding to $A_0=0.915$ evolved to a saturated 3-D flow with $A=0.897$. Using the values of α_1 , Re_c , and the asymptotic amplitudes A from the nonlinear calculations, we constructed the bifurcation diagram shown in the inset to Fig. 3(a). This diagram is necessarily schematic because the data do not permit a reliable estimate of the coefficient of the quintic term in the normal form. This term is responsible for the saturation of the time series in Fig. 3(a) and the turning point in the bifurcation diagram. Precise determination of this coefficient is left to future work. However, the correct prediction of final states by the normal form with the estimated coefficients and the demonstration of bi-stability for $Re < Re_c$ confirms that the bifurcation is subcritical.

Figure 4 illustrates the asymptotic 3-D flow at $Re=195$, similar to experimental flow visualization above Re_c . From the initial superposition $\mathbf{U} + \tilde{\mathbf{u}}_c$, the flow has developed a complex three-dimensional vorticity field with significant streamwise vorticity far downstream. In this saturated state the wake is 3-D and time-periodic, but with a slightly lower shedding frequency. It is unknown whether this flow is stable to further 3-D perturbations, but experimental evidence suggests it is not.⁵

Our finding of a subcritical secondary instability is consistent with experimental observations,⁶ but stands in contrast to other computational studies which conclude that the bifurcation is supercritical. Karniadakis and Triantafyllou⁷ find a soft transition and stable 3-D solutions for Reynolds numbers up to 225, but these calculations are for narrow domains ($L = \pi/2$ diameters) and do not correspond to the instability considered here. Zhang *et al.*⁸ have studied the evolution of disturbances in domains with spanwise lengths

of $L=6$ to 18 diameters. They report both hard *and* soft transitions, although only the latter is relevant to the discussion here (the hard transition is observed at $Re \approx 160$ and does not correspond to a bifurcation from the 2-D flow). The soft transition occurs at $Re \approx 180$ and produces a 3-D flow that agrees qualitatively with Fig. 4. While this transition is attributed to supercritical behavior, they do not report growth rates or 3-D results in the small hysteretic range of Re found here. Noack and Eckelmann⁹ provide indirect evidence of a supercritical bifurcation in a low-dimensional model of the 3-D wake. However, the critical values computed from their model compared to our results are 10% lower in Reynolds number and 45% higher in wave number. Given the immense computational requirements necessary for full resolution of the cylinder wake, it is not surprising that previous computations failed to detect weak subcriticality.

In summary, we performed a combined linear and nonlinear computational study of secondary instability in the wake of a circular cylinder. From our linear stability calculations we determined the precise critical values for the 3-D instability of the 2-D wake. Using full 3-D simulations near the critical point, we estimated the Landau constant for this bifurcation and provided the first clear numerical evidence that the secondary instability is subcritical. These calculations firmly establish the nature of the secondary instability for an infinitely long cylinder in an open flow.

ACKNOWLEDGMENTS

R.D.H. acknowledges support from ONR Grant No. N00014-94-1-0793 and NSF Grant No. CDA-9318145. D.B. acknowledges support from the Nuffield Foundation and NSF Grant No. DMS 92-06224. Our 3-D simulations were performed in part using the Intel Paragon System operated by Caltech on behalf of the Concurrent Supercomputing Consortium. Access to this facility was provided by the California Institute of Technology.

¹C. P. Jackson, "A finite-element study of the onset of vortex shedding in flow past variously shaped bodies," *J. Fluid Mech.* **182**, 23 (1987).

²G. Mathis, M. Provansal, and L. Boyer, "Bénard-von Kármán instability: Transient and forced regimes," *J. Fluid Mech.* **182**, 1 (1987).

³D. Barkley and R. D. Henderson, "Three-dimensional Floquet stability analysis of the wake of a circular cylinder," to appear in *J. Fluid Mech.*

⁴J. Guckenheimer and P. Holmes, *Nonlinear Oscillations, Dynamical Systems, and Bifurcations of Vector Fields* (Springer, New York, 1983).

⁵C. H. K. Williamson, "Mode A secondary instability in wake transition," *Phys. Fluids* **8**, 1680 (1996).

⁶C. H. K. Williamson, "The existence of two stages in the transition to three dimensionality of a cylinder wake," *Phys. Fluids* **31**, 3165 (1988); T. Leweke and M. Provansal, "The flow behind rings—bluff-body wakes without end effects," *J. Fluid Mech.* **288**, 265 (1995).

⁷G. E. Karniadakis and G. S. Triantafyllou, "Three-dimensional dynamics and transition to turbulence in the wake of bluff objects," *J. Fluid Mech.* **238**, 1 (1992).

⁸H.-Q. Zhang, U. Fey, B. R. Noack, M. König, and H. Eckelmann, "On the transition of the cylinder wake," *Phys. Fluids* **7**, 779 (1995).

⁹B. R. Noack and H. Eckelmann, "A global stability analysis of the steady and periodic cylinder wake," *J. Fluid Mech.* **270**, 297 (1994).